J Mater Sci: Mater Electron (2017) 28:595–600
DOI 10.1007/s10854-016-5563-5

CrossMark

Dielectric–electrode interactions in glass and silicon-compatible thin-film (Ba,Sr)TiO_3 capacitors

Saumya Gandhi[1] · Shu Xiang[1] · Manish Kumar[1] · Himani Sharma[1] · Parthasarathi Chakraborti[1] · P. Markondeya Raj[1] · Rao Tummala[1]

Received: 13 June 2016 / Accepted: 16 August 2016 / Published online: 6 September 2016
© Springer Science+Business Media New York 2016

Abstract This paper investigates the role of electrode–dielectric interactions, and barrier materials on leakage current, breakdown voltage, yield and reliability of thin-film (Ba,Sr)TiO_3 capacitors on silicon and glass substrates. The first part of the paper investigates the electrode–dielectric interactions with sputtered Cu and Ni electrodes to identify the mechanisms that lead to high leakage current and low yield. The second part of the paper presents lanthanum nickel oxide as a viable solution to overcome the problems with sputtered Cu and Ni electrodes. A combination of low leakage current, high yield and capacitance densities was achieved with the oxide electrode systems.

1 Introduction

Packaging has evolved from plastic to ceramic and, more recently, to organic packages. Silicon and glass packages are being developed as the next generation packages with higher I/O density [1]. They need to be enhanced as well for power integrity by means of lower power-ground impedance for enhancing electrical performance [2–5]. Decoupling capacitors are typically used along the power distribution network to lower the impedance across a broad frequency band that covers all the IC switching operations. This has been achieved traditionally through surface-mount devices (SMDs) onto PWBs fabricated with multilayer ceramic capacitors. These decoupling capacitors, however, only address low-frequency switching noise, necessitating the use of on-chip decoupling for higher frequencies. While on-chip decoupling is very effective with capacitors in ICs, this is a very expensive approach. Integrating decoupling capacitors as thinfilms in high-performance interposers or packages, is another option that can lead to low power supply noise and improved power integrity, particularly if these capacitors can be very close to the transistors. These benefits are thus enabled by ultra-short interconnect distances between the capacitor and the active chip leading to lower parasitic inductances and resistances [6, 7].

Thin films with high capacitance can be achieved with high-permittivity dielectrics. Barium strontium titanate (BST) and barium titanate (BT) with permittivities in the range of 200–500 are preferred candidates for thinfilm capacitors. They have no major toxicity concerns that are associated with lead-based perovskites such as lead zirconate titanate (PZT). The electrical properties, defect density and long-term reliability of sputtered BST films depend on sputtering power, chamber pressure, BST composition, post-annealing process and the bottom electrode system [8, 9]. BST is usually crystallized at temperatures of above 700 °C. Glass-based capacitor integration, however, requires processing temperatures of below 700 °C due to the glass-softening at this temperature and above. These films have not been successfully integrated on glass because of the processing challenges associated with crystallizing such films at high temperatures of around 700 °C.

High-permittivity thinfilm capacitors on silicon have been widely investigated but primarily with Pt electrodes using titanium, or tantalum as the diffusion barriers and adhesion promoters between Pt and Si. However, these systems have many limitations including long-term

✉ P. Markondeya Raj
pm86@mail.gatech.edu

[1] Packaging Research Center, Georgia Institute of Technology, 813 Ferst Drive, Atlanta, GA 30332-0560, USA

electrical fatigue, loss in polarization, inadequate adhesion, and high cost. These limitations have driven researchers to find alternative electrode systems such as copper and nickel [10]. Because of their relatively low melting points compared to Pt, base metal electrodes such as copper or nickel undergo recrystallization and grain growth during the heat treatment at temperatures as low as 450 °C, resulting in rough metal-oxide interfaces [11]. In addition, these electrodes are more prone to oxidation during the dielectric crystallization processes, resulting in diffusion into the dielectrics or substrates [12]. This leads to microcracks and voids, which result in high current leakage, low BDV and low process yield. It is, therefore, important to identify and study suitable diffusion barriers between the electrodes, dielectrics and substrates, and optimize the post-annealing processes to minimize these detrimental interfacial reactions to improve the overall capacitor performance.

Various kinds of barriers were investigated to address the electrode instabilities with copper and nickel electrodes. On the silicon side, a double-barrier of Ta/TaN was found to be effective in suppressing the copper diffusion [13]. Alternatively, an alloy of Cu–Mn was also found to suppress copper migration as the Mn migrates first into the silicon interface to form thin barrier oxides [14]. TiAl has been explored as a barrier at the Cu/dielectric interfaces, to prevent interfacial reactions. In most of these approaches, a thin interfacial reaction layer, which acts as an additional dielectric layer, forms between the metal and BST [11]. This interfacial layer dilutes the overall capacitance density of the dielectric films.

Conductive metal-oxide electrodes such as lanthanum nickel oxide (LNO) are most suitable replacements for Cu and Ni metal electrodes because of their stability in high temperature and oxygen atmospheres. They also suppress the interfacial reactions, and act as sinks for the entrapment of defects [15, 16]. LNO forms a perovskite oxide electrode that goes one step beyond by providing a lattice-matched structure with the perovskite dielectrics, thus minimizing the CTE mismatch. Hence, they are more ideally suited for enhancing the reliability of the dielectrics by remaining stable at the high (>600 °C) annealing temperatures.

The goal of this paper is to investigate dielectric–electrode interactions with BST as a dielectric and copper and nickel as electrodes. Another goal of this paper is to apply this learning with a different electrode system such as LNO, using a low-cost chemical synthesis approach that overcome the problems with sputtered Cu and Ni electrodes. The role of electrode instabilities on dielectric characteristics and yield are studied to obtain optimal process conditions for each system.

2 Experimental methods

Two types of substrates, 200-micron thickness glass and 500-micron thick silicon wafers were used in this study. Silicon substrates were coated with a 500 nm layer of silicon oxide followed by a 200 nm layer of silicon nitride. Borosilicate glass substrates were used as received.

Both metal and conducting oxides were used as electrodes in this study. The metal electrodes were formed by sputter-depositing an adhesion layer (20 nm), followed by sputter-deposition of Cu or Ni as the electrode layers (500 nm). Tantalum was chosen as the adhesion layer. It also acts as a diffusion barrier between the electrode and silicon. Copper was sputtered at 1000 W (2.5 A, 400 V) with a 6-inch target to give a deposition rate of 8 A/s. Nickel and titanium were deposited at 350 W (1.35 A, 260 V) with a 3-inch target at a deposition rate of 1–2 A/s.

Conducting oxide electrode films made of LNO were utilized as the second electrode system. ZrO_2 was used as the barrier between the oxide electrode and the substrate because of its known effectiveness as a diffusion barrier to suppress any chemical interactions between the substrate and electrode. The conducting oxide LNO was prepared by dissolving lanthanum nitrate and nickel acetate in methoxy ethanol to form a 0.1 M solution. In order to ensure complete dissolution of the precursors with good homogeneity, the solgel solutions were refluxed at 125 °C for 6 h after each precursor was added. The sol–gel derived LNO films were deposited onto the substrates using spin-coating for 30 s at 4000 RPM (rotations per min). The coated samples were heated on a hot-plate at 400 °C for 5 min to evaporate the solvents and also pyrolyze the organic content. Multiple coatings were applied in order to increase the thickness and resultant conductivity. After achieving the desired thickness, the samples were post-annealed in an oxygen rich atmosphere to crystallize the LNO.

BST dielectric was then deposited using RF sputtering in a 60:40 O_2:Ar atmosphere. Dielectric films of 75–300 nm were deposited at 75 W. The films were post-annealed at 700 °C for 30 min. A slow ramp rate of 5 °C/min was used for the annealing process. In case of the metal electrodes, an inert nitrogen atmosphere was used. However, with LNO as the bottom electrode, an oxygen-rich atmosphere was employed to crystallize the BST. A 200-nm gold layer was deposited using a shadow mask to form the top electrode. X-ray Diffraction (XRD), Scanning Electron Microscopy (SEM) and X-ray Photoelectron Spectroscopy (XPS) were used to characterize the films.

The capacitors were then tested using a LCR meter. HP 4285A precision LCR meter was used for C–V measurements. A 1-V AC signal was applied for the capacitance measurements. Leakage current analysis was performed

with Keithley 6485 picoammeter. A voltage increment of 0.5 V was used for the leakage current measurements.

3 Results and discussion

3.1 Structural characterization

The X-ray diffraction patterns of sintered BST films crystallized at 700 °C are shown in Fig. 1, depicting the perovskite structure of polycrystalline BST films. Gold (Au) peaks from the top electrode are also visible in the XRD pattern because the same samples were used for electrical and structural characterization. XRD analysis of the thin film showed that all the BST peaks are more intense at higher sintering temperatures, implying higher degree of crystallinity. A small amount of pyrochlore phase is detected in some cases, as evident from the characteristic 29° peak. In the spectra with metal electrodes, extraneous peaks from metal oxides were also detected.

The films sputtered on copper showed cracks as observed in the SEM images from Fig. 2a and b. The cracks in the BST resulted in high leakage currents, poor yield and reliability. These cracks are attributed to the instabilities in the copper electrode due to stress-relief under annealing, recrystallization and grain growth. The cracks also provide a diffusion path for oxygen to reach the copper interface, resulting in subsequent oxidation of the copper. Cu^{+} ions are known to diffuse through the dielectric to the surface where they get oxidized. The diffusion is aggravated through grain boundaries, pin-holes and other defects in the dielectric. This phenomenon results in an outward oxide growth that eventually forms hillocks [11]. Hillock formation is also feasible in the absence of oxygen, just from the stress-relief from annealing, grain coarsening or recrystallization [17]. When hillocks form, the average roughness varies from 50 to 120 nm. The motion of Cu^{2+} to the surface also results in voids, as evident in Fig. 2c. Tantalum diffusion to the surface has also been observed. This is attributed to the high affinity of Ta for oxygen.

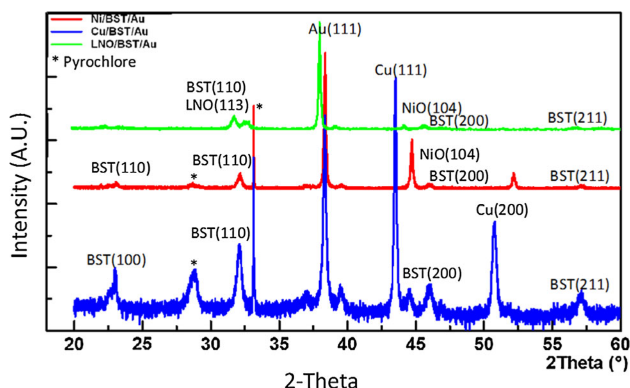

Fig. 1 XRD patterns of BST dielectrics with Cu, Ni and LNO electrodes

In the absence of a barrier between Si and Cu, Cu diffuses into Si and also reacts with the Si at the elevated post-anneal temperatures to form Cu_3Si and subsequently to SiO_2 when exposed to oxygen rich atmospheres [18]. Ta prevents this Cu interdiffusion and interfacial reaction to some extent while TaN is found to be more effective. Previous studies have demonstrated copper movement along grain boundaries of the Ta when Ta is used as a barrier [11, 13].

With films sputtered on Ni electrodes, the hillocking effect was partially suppressed because of the relatively stable electrode structure, suppressed nickel oxidation and interdiffusion, but still sufficient enough to cause cracks in the films and high leakage when the temperature exceeds 650 °C. The SEM image in Fig. 2d shows the presence of cracks due to the nickel-BST interdiffusion and nickel grain growth. This effect is more predominant when the annealing temperature exceeds 750 °C.

The BST films sputtered on LNO/ZrO_2/Si did not show such cracks or heterogeneous grain structure arising from grain growth and recrystallization as is evident in Fig. 3. The films showed high yield and low leakage current as compiled in Table 1. The LNO forms a stable chemical interface with minimal interfacial reactions and lattice-matched structure as discussed in Sect. 1.

An XPS depth-profile analysis was conducted to compare the BST interdiffusion distances with Pt, Ni and Cu electrodes. The interdiffusion plots for oxygen and the electrode metal (Pt, Ni (LNO), Ni, and Cu) are shown in Fig. 4a and b respectively. The analysis clearly shows a diffuse interface between the electrode and BST film where the atomic percentages of oxygen stays constant for the dielectric film thickness and gradually decreases with etch-time (representing thickness) when the electrode interface is reached. The distance over which the ions interdiffuse is indicated by the number of etch steps when the concentration gradients are observed. Since the etch rate for the interdiffusion zone varies with each system, only a qualitative comparison can be obtained from the etch-time or the number of etch steps. The smallest oxygen interdiffusion distances are seen for Pt, followed by Cu and Ni. Similarly, the same trend is observed for the electrode interdiffusion distances. The XPS analysis clearly indicates significant interdiffusion with Cu and Ni compared to Pt. The interdiffusion between LNO and BST is much lower compared to Cu and Ni, as seen in Fig. 6b. In a previous Cu/BST interdiffusion study with XPS depth-profiling by Kim et al., copper ions were found to diffuse into the

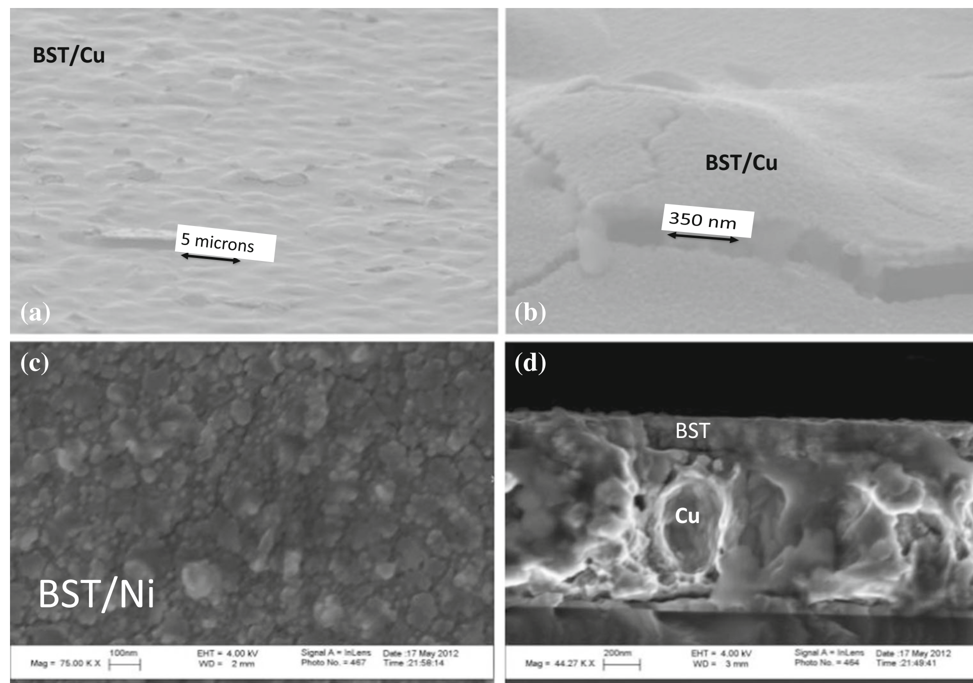

Fig. 2 SEM images showing instabilities in BST/Cu and BST/Ni after high temperature anneal at 700 °C. **a** Large hillocks formed on the BST surface with Cu as the bottom electrode. **b** Large cracks are evident on the BST surface as a result of hillocks. **c** A cross-section SEM image showing voids in the Cu and **d** cracks in the BST film with Ni as bottom electrode and nickel oxide phases on the surface

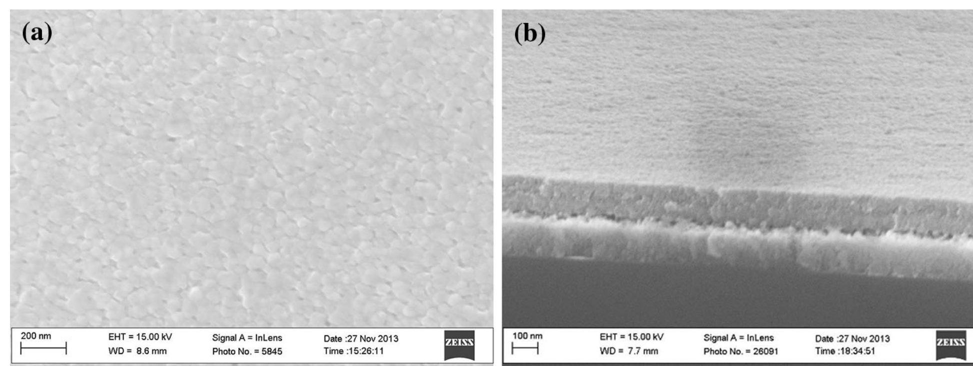

Fig. 3 SEM images of sputtered BST on LNO electrodes. **a** Surface morphology of BST on LNO electrode and **b** cross-section of BST on LNO showing sharp interfaces—indicating no inter-diffusion between the layers

Table 1 Electrical properties and yield with different electrode systems

	Metal electrodes		Conducting oxide electrode
	Ta/Cu/BST	Ta/Ni/BST	ZrO_2/LNO/BST
Annealing conditions	700 °C, 30 min in N_2	700 °C, 30 min in N_2	700 °C 30 min in O_2
Capacitance density	7–8 nF/mm^2	9–11 nF/mm^2	15–20 nF/mm^2
Leakage current at 3 V	10–20 µA/mm^2	1–1.5 µA/mm^2	30–40 nA/mm^2
Yield	40 % (14/35 devices yielded)	57 % (20/35 devices yielded)	95 % (33/35 devices yielded)

dielectric at 200 °C but no substantial diffusion was seen at 100 °C. The interdiffusion zone acts as a dead-layer with low capacitance and also provides sources for traps that increase the leakage current. Therefore, lower capacitance and higher leakage currents are seen with Cu and Ni, as described in the next section.

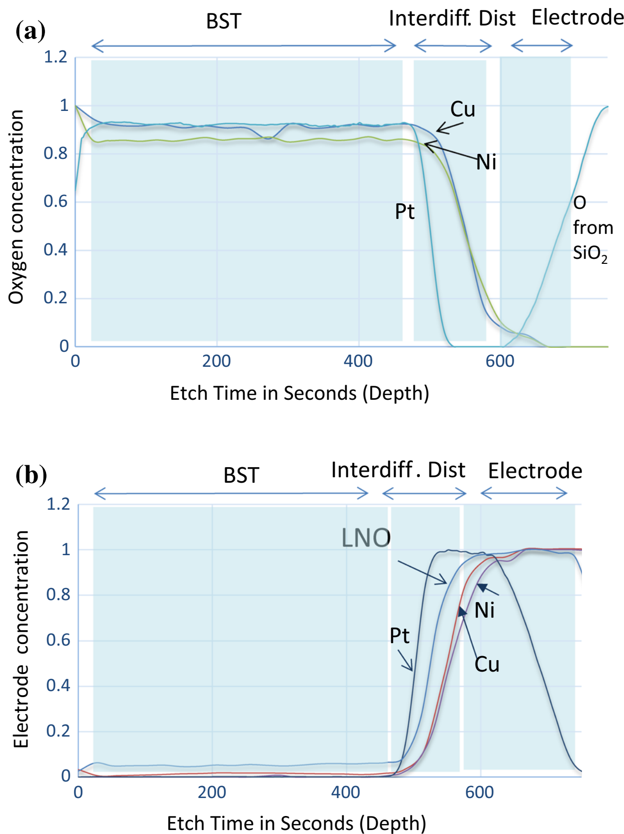

Fig. 4 XPS compositional depth profile of BST films with various electrodes: **a** oxygen concentration gradient and **b** electrode concentration gradient

3.2 Electrical characterization

3.2.1 Platinum, copper and nickel electrodes

The first set of electrical measurements were performed with BST films on Pt electrodes. After BST deposition, post-annealing was performed at 700 °C in the presence of nitrogen. Capacitance densities of ~20 nF/mm^2, corresponding to a dielectric constant of >~450 was achieved with Pt electrodes at an annealing temperature of 700 °C. The electrical properties of the BST capacitors from various electrode systems are shown in Table 1. In comparison, a lower capacitance density of 7 nF/mm^2 was achieved for BST/Cu/Ta/SiN/Si planar system. The Cu and BST film thicknesses were ~500 and ~200 nm respectively. The capacitance density, therefore, corresponds to an effective permittivity of ~158. High leakage currents of ~10–20 μA/mm^2 (Fig. 6) with this system are consistent with the SEM images from Fig. 2. The capacitance densities and leakage currents with BST/Ni/Ta/SiN/Si systems are 10 nF/mm^2 (corresponding to an effective permittivity of 227) and 1.5 μA/mm^2 respectively, much improved than those from the copper electrodes.

The BST films on Cu electrodes depicted an opposite trend in capacitance densities with annealing temperatures compared to platinum electrodes. With increasing crystallization temperatures, the capacitance values decreased. Films annealed at temperatures of 550 °C (9–10 nF/mm^2) depicted higher permittivities over those annealed at 700 °C (7 nF/mm^2). This trend results from the formation of an interface dead-layer of metal oxide between the BST dielectric and base metal electrode. The formation of the dead-layer results in an overall decrease in permittivity. A simple model with two capacitors in series, as seen in Fig. 5, can be used to explain the lower permittivity. In the figure, C_{ideal} is the capacitance obtained from a BST film of thickness 200 nm on Pt electrodes. C_{tot} is the capacitance obtained with Cu or Ni electrodes with a BST film of same thickness. This representation can estimate the capacitance from the dead-layer ($C_{Cu/BST}$ or $C_{Ni/BST}$), formed from the interfacial reactions between the BST dielectric film and the base metal electrode. It is clear from the equation that the effect of the dead-layer capacitance will be more dominant for thinner BST layers and thicker oxide layers.

$$C_{\mathrm{Interface}} = \frac{C_{\mathrm{ideal}} \times C_{\mathrm{tot}}}{C_{\mathrm{ideal}} - C_{\mathrm{tot}}} \quad (1)$$

Assuming that the BST has the same permittivity as that on Pt electrodes, the estimated interface dead-layer and film capacitances for Cu electrodes are 10.7 nF/mm^2, while those with Ni electrodes are 20 nF/mm^2.

The leakage current data on base metal electrodes also demonstrated opposite behavior to that seen on Pt electrodes. BST films on Pt electrodes have reduced leakage currents and dielectric loss after high temperature post-annealing. However, in the case of Cu or Ni electrodes, an increase in both leakage current and dielectric loss has been observed. This can be attributed to the significant grain growth that is observed after post-annealing at temperatures of 700 °C. This grain growth and subsequent hillock formation is more evident in copper compared to nickel as discussed in the previous sections. Consistent with the observed microstructures, higher leakage current and losses were observed in BST films on Cu compared to those grown on Ni. The aforementioned effects also affect the overall capacitor yield. As is evident from the data in

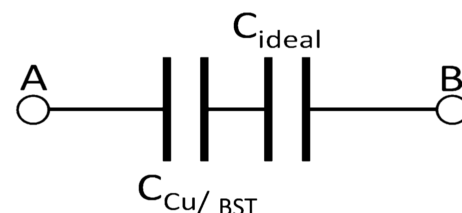

Fig. 5 Series capacitor structure formed because of the interface dead-layer between BST and the base metal electrode (Cu or Ni)

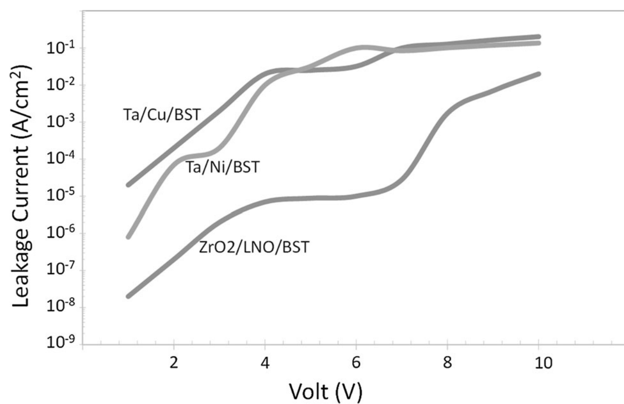

Fig. 6 Leakage current plots for Cu, Ni and LNO electrodes

Table 1, BST films on Cu had the lowest yield ∼40 %, whereas Ni had a yield of almost 60 %.

3.2.2 Lanthanum nickel oxide

The electrical performance of capacitors with Cu and Ni-based electrodes was compared to that from LNO electrodes deposited on Si with ZrO_2 film as the barrier. Capacitors formed using LNO as the bottom electrode showed superior properties relative to those prepared with Cu and Ni. With LNO/ZrO_2/Si as the bottom electrode, capacitance density was found to be 15–20 nF/mm^2 (corresponding to a permittivity of 455) with 95 % yield, as shown in Table 1. The LNO/BST electrode–dielectric system formed crack-free films with lower interdiffusion evident from the sharp interfaces between the electrode and dielectric compared to those with Cu and Ni as seen in Fig. 6. LNO diffusion into the silicon is presumably suppressed by using zirconia as the barrier. Higher capacitance density and relatively lower leakage current values compared to the Cu and Ni systems are attributed to stable interfaces and crack-free films. A comparison of the leakage current data obtained from Cu, Ni and LNO electrodes is plotted in Fig. 6. The surface roughness and inhomogeneous microstructure contributes to the leakage currents. With smooth LNO films from improved sol–gel process, the electrical performance can be further improved. The capacitance density and leakage current were found to be similar to those with Pt electrodes.

4 Conclusions

Capacitance density and leakage current characteristics of thinfilm capacitors on silicon and emerging glass substrates were investigated with two different electrode systems; base metals such as Cu or Ni and conductive oxides such as LNO. With sputtered copper metal electrodes, the electrode–dielectric interactions create macroscopic and microscopic defects in the dielectrics after annealing. This results in poor electrical performance and yield, thus requiring electrode stabilization and suitable barriers between the metal-dielectric and metal-substrate interfaces. Nickel electrodes, on the other hand, showed lower leakage currents and higher capacitance densities. The instabilities in this case are related to hillock formation during thermal stress relief, oxygen diffusion and recrystallization. These instabilities are more predominant with copper electrodes compared to nickel. Conducting oxide electrodes, on the other hand, showed stable interfaces resulting in higher capacitance densities of up to 20 nF/mm^2 and lower leakage currents of 30 nA/mm^2 (at 3 V). This is attributed to the improved thermal and interfacial stability of these electrodes, making this a viable technology for integrating thinfilm decoupling capacitors in silicon and glass interposers and packages.

References

1. R.R. Tummala, M. Swaminathan, M.M. Tentzeris et al., IEEE Trans. Adv. Packag. **27**, 250 (2004)
2. G. Kumar, T. Bandyopadhyay, V. Sukumaran, V. Sundaram, S.K. Lim, R. Tummala, Electronic Components and Technology Conference (ECTC), 2011 IEEE 61st IEEE (2011)
3. V. Sukumaran, T. Bandyopadhyay, Q. Chen, et al., Electronic Components and Technology Conference (ECTC), 2011 IEEE 61st IEEE (2011)
4. V. Sukumaran, T. Bandyopadhyay, V. Sundaram, R. Tummala, IEEE Trans. Comp. Packag. Manuf. Technol. **2**, 1426 (2012)
5. V. Sukumaran, Q. Chen, F. Liu, et al., Electronic Components and Technology Conference (ECTC), 2010 Proceedings 60th IEEE (2010)
6. L.D. Smith, R.E. Anderson, D.W. Forehand, T.J. Pelc, T. Roy, IEEE Trans. Adv. Packag. **22**, 284 (1999)
7. M. Swaminathan, J. Kim, I. Novak, J.P. Libous, IEEE Trans. Adv. Packag. **27**, 286 (2004)
8. P. Padmini, T. Taylor, M. Lefevre, A. Nagra, R. York, J. Speck, Appl. Phys. Lett. **75**, 3186 (1999)
9. A. Ianculescu, B. Despax, V. Bley, T. Lebey, R. Gavrilă, N. Drăgan, J. Eur. Ceram. Soc. **27**, 1129 (2007)
10. J.N. Reck, R. Cortez, S. Xie, M. Zhang, M. O'Keefe, F. Dogan, Appl. Surf. Sci. **258**, 5599 (2012)
11. W. Fan, B. Kabius, J. Hiller et al., J. Appl. Phys. **94**, 6192 (2003)
12. J.S. Kim, M.G. Kang, S.H. Kweon et al., J. Am. Ceram. Soc. **96**, 1248 (2013)
13. K. Holloway, P.M. Fryer, C. Cabral Jr., J. Harper, P. Bailey, K. Kelleher, J. Appl. Phys. **71**, 5433 (1992)
14. J. Koike, M. Wada, Appl. Phys. Lett. **87**, 041911 (2005)
15. Y. Wang, S. Xiang, P.M. Raj, H. Sharma, B. Williams, R. Tummala, Electronic Components and Technology Conference (ECTC), 2011 IEEE 61st IEEE (2011)
16. H. Suzuki, Y. Miwa, T. Naoe et al., J. Eur. Ceram. Soc. **26**, 1953 (2006)
17. C.-L. Dai, F.-Y. Xiao, C.-Y. Lee, Y.-C. Cheng, P.-Z. Chang, S.-H. Chang, Mater. Sci. Eng. A **384**, 57 (2004)
18. N. Fréty, F. Bernard, J. Nazon, J. Sarradin, J.-C. Tedenac, J. Phase Equilib. Diffus. **27**, 590 (2006)